LMA fibers modal decomposition using image factor analysis

Jean-Joseph Max, Bertrand Gauvreau, Benoit Sévigny, Mathieu Faucher
ITF Laboratories, 400 Montpellier Blvd., Montréal, Québec, H4N 2G7 Canada

ABSTRACT

A new method is presented for the analysis of the modal content of a beam travelling in a waveguide. This method uses a simple optical set up to record beam images. Depending on the application, the source can be broad band (BBS) or a tunable laser. The method uses the eigenmode profiles of the waveguide under test, either theoretical or experimental ones. In this case, the technique is applied to characterize the modal content of few moded large mode area (LMA) fibers. Such LMA fibers are typically used in high power fiber lasers and amplifiers to reduce sensitivity to non-linear effects. By calculating the scalar products of the unfolded experimental and theoretical 2D profiles, the modal content is obtained. Access to such cost effective and easy to implement diagnosis tool will greatly help improving modal quality preservation in components and systems based on the fundamental mode operation of few moded LMA fibers. The high precision and performance of the method is evaluated using both computer generated and experimental data sets.

Keywords: LMA fiber, device modal quality, transmission.

1. INTRODUCTION

Because non linear effects increase strongly with increasing power transport in waveguides, the most useful remedy is to increase the guiding area by increasing the fiber core diameter.[1] LMA permit to increase the core damage threshold and suppress unwanted nonlinear loss processes. For this reason, LMA fibers are now key components of high power fiber lasers and amplifiers. However, due to their increased core diameter, LMA fibers are guiding several higher-order modes (HOM) that decrease beam quality by, among others: (i) increasing the divergence of the beam[1] and (ii) producing modal interferences that vary with wavelength and fiber length.[2,3,4] Hence, special care must be taken in the fabrication process of devices using LMA to keep these close to single mode operation, namely by using mode field adapters (MFA) to launch a singlemode source into LMA fibers and the reverse.[5]

Accurate evaluation of the modal content at the output of multimode fiber devices is required in many applications that rely on fiber output beam quality, in order to determine the power distribution within the first lower order modes.[6] The usual beam quality factor of an optical beam is given by the ratio of divergence of the beam to that of the theoretical first order Gaussian equivalent one.[1] This is called the M^2 parameter. This beam quality measurement method is not well adapted for small sized and highly diverging fiber laser sources. They usually need to be collimated first and re-imaged again to produce a secondary waist that can then be analyzed. Modal interferences also bring beam size variation and pointing errors during the waist measurement, leading to inaccurate M^2 evaluation. Therefore, low M^2 values do not guarantee low HOM content. [2,3,4,7] A more recent method performs a spectrally and spatially resolved imaging (S^2I).[3,6,7] This method is useful to qualitatively observe HOM propagation and excitation in an optical device. However, S^2I has some theoretical and practical flaws. On a theoretical point of view: (i) two or more eigenmodes may propagate with similar velocities that will not be properly be distinguished by S^2I; (ii) eigenmode velocity difference varies with wavelength distorting the results (depending on the wavelength range used for S^2I); (iii) eigenmode velocity of two modes may cross in a small wavelength range which reduces the accuracy of the results; (iv) this analysis method is valid as long as most of the optical power is carried by one mode (the fundamental one) which may restrict its use; (v) simulations revealed strong limitations in accuracy for low intensity HOM (in opposition to point iv). On a practical point of view, it requires either a wavelength scan or beam image scan with the use of a spectrometer. It can also require an unpractical length (tens of meters) of fiber in order to discriminate the modes. Other attempts to extract the mode components in beam intensities based on independent component analysis using either theoretical or experimental mode far field profiles have also been proposed.[8,9]

In the present work, we apply factor analysis (FA) to the near field beam profile at the output of LMA fibers. Knowing the physical properties of the LMA used, namely its core diameter and numerical aperture (NA) and/or its refractive index profile (RIP), the mode theoretical field profiles can be calculated and further used for independent beam components in the FA process. Having access to the quantitative modal content right at the output of the LMA fiber

provides a complete beam characterization and theoretical calculation of beam characteristics such as M^2 and pointing error can be successively derived.

2. THEORY

2.1 Factor analysis

FA of a data set is a procedure by which the principal factors (components) of an evolving system can be identified and their relative weights obtained from derived multiplying factors (MFs).[10] FA is a powerful method that was successfully used to study many chemical systems using infrared spectroscopy,[11-15] and can also be used to obtain the modal distribution of power in the output beam from a given optical fiber. The modal content of a beam propagating in an optical fiber is represented by the power distribution within the eigenmode basis for this fiber.[8] Each eigenmode produces a well defined field (power) profile on the output surface of the fiber that can be theoretically captured from the physical parameters of the output fiber. S^2I is using this property to sort out the propagating modes and evaluate their respective power by analyzing the beam image variations with wavelength.[3] This method of modal analysis suffers from theoretical limitations such as multimode interferences as well as numerical limitations among these: frequency leakage related to the frequency sampling used that may not properly match the mode interference beating period. In the proposed method, each eigenmode is associated with a single eigenimage that represents the related field amplitude and energy spatial distribution. Therefore, the eigenmode basis is directly associated with an eigenimage basis that can be used in an image factor analysis (IFA) process. The only remaining task is to determine the multiplying factors (MFs), that is: the weigh of each of the elements of the factor basis.

2.2 Image factor analysis

An effective FA procedure had recently been proposed to determine, in a spectral set, the number of principal factors, their spectra, and their MFs.[12] The first step in the procedure is to determine the number of principal factors. In the present case, by solving the propagation equations, the number of modes and the corresponding eigenmode basis are determined. LMA fibers may support numerous modes that are more or less excited or are lost due to fiber bending and others physical constraints. We therefore restrict the analysis to a few propagating modes. IFA basic equations are taken from ref. 12. The principle is the following: the fiber beam images are made of (x, y) pixels; each image of a set of n images $\mathbf{B}$ (x, y, n) is assumed to be a linear combination of the eigenmode images $\mathbf{M^P}$ at given relative power (or multiplying factors: MFs). This is formalized as:

$$\left(\mathbf{B}\right)_{x,y,n} = \left(\mathbf{M^P}\right)_{x,y,f} \times \left(\mathbf{MF}\right)_{f,n} + \left(\mathbf{R}\right)_{x,y,n}, \tag{1}$$

Where f is the number of eigenmodes and $\mathbf{R}$ are the residues from factor analysis. Equation (1) is using a pseudo matrix notation that directly follows the one used for FA in the spectroscopic domain. The spectra are two dimensional ones (intensity against frequency) whereas the images are three dimensional (intensity over the plane). In the matrix notation used in the present work, the three dimensional images with dimension I(x, y) are unfolded by downwards concatenation of the matrix columns giving vectors of length $x \times y$. Keeping in mind this implicit writing, we use the same notation as in ref. 12 for simplicity, defining the two dimensional (x, y) "scalar" product as an extension of the usual one: multiplication of the two matrices term by term and summing the result over the two dimensions. This is equivalent to the usual scalar product after unfolding the two dimensional matrices into a vector. The basic criterion of validity for eq. (1) is the overall amplitude of residue $\mathbf{R}$ which should be almost zero.

Multiplying each term of Eq. (1) by the "transpose" of the eigenmode matrix $\left(\mathbf{M^P}\right)^{\mathrm{T}}_{f}$ gives:

$$\left(\mathbf{M^P}\right)^{\mathrm{T}}_{x,y,f} \times \left(\mathbf{B}\right)_{x,y,n} = \left(\mathbf{M^P}\right)^{\mathrm{T}}_{x,y,f} \times \left(\mathbf{M^P}\right)_{x,y,f} \times \left(\mathbf{MF}\right)_{f,n} + \left(\mathbf{M^P}\right)^{\mathrm{T}}_{x,y,f} \times \left(\mathbf{R}\right)_{x,y,n} \tag{2}$$

Further multiplying the terms of Eq. (2) by the inverse matrix of the "scalar products" of the eigenmode matrix $\left[\left(\mathbf{M^P}\right)^{\mathrm{T}}_{x,y,f} \times \left(\mathbf{M^P}\right)_{x,y,f}\right]^{-1}_{f,f}$ yields:

$$\left[\left(\mathbf{M^P}\right)^{\mathrm{T}}_{x,y,f} \times \left(\mathbf{M^P}\right)_{x,y,f}\right]^{-1} \times \left(\mathbf{M^P}\right)^{\mathrm{T}}_{x,y,f} \times \left(\mathbf{B}\right)_{x,y,n} = \left(\mathbf{MF}\right)_{f,n} + \left[\left(\mathbf{M^P}\right)^{\mathrm{T}}_{x,y,f} \times \left(\mathbf{M^P}\right)_{x,y,f}\right]^{-1} \times \left(\mathbf{M^P}\right)^{\mathrm{T}}_{x,y,f} \times \left(\mathbf{R}\right)_{x,y,n} \tag{3}$$

From Eq. (3) one obtains the multiplying factor matrix $(\mathbf{MF})_{f,n}$:

$$(\mathbf{MF})_{f,n} = \left[(\mathbf{M^P})^{\mathrm{T}}_{x,y,f} \times (\mathbf{M^P})_{x,y,f}\right]^{-1} \times (\mathbf{M^P})^{\mathrm{T}}_{x,y,f} \times (\mathbf{B}\ )_{x,y,n} - \left[(\mathbf{M^P})^{\mathrm{T}}_{x,y,f} \times (\mathbf{M^P})_{x,y,f}\right]^{-1} \times (\mathbf{M^P})^{\mathrm{T}}_{x,y,f} \times (\mathbf{R}\ )_{x,y,n} \quad (4)$$

In equation (4), there are three "scalar product" matrices: (i) the "scalar products" of the eigenmode images with themselves: $\left[(\mathbf{M^P})^{\mathrm{T}}_{x,y,f} \times (\mathbf{M^P})_{x,y,f}\right]$; (ii) the "scalar products" of the eigenmode images with each of the experimental images: $(\mathbf{M^P})^{\mathrm{T}}_{x,y,f} \times (\mathbf{B}\ )_{x,y,n}$; and (iii) the "scalar products" of the eigenmode images with each of the residue images: $(\mathbf{M^P})^{\mathrm{T}}_{x,y,f} \times (\mathbf{R}\ )_{x,y,n}$.

The primary challenge of FA is to sort out the principal components, that is: the eigenmode images. This difficulty is avoided (i) since the fiber characteristics are known and the eigenmode can be accurately calculated or (ii) since every eigenmode is guided by the same fiber, only 2 (3) parameters are required to generate the eigenmode basis set, namely: the fiber core radius and fiber numerical aperture and/or the refractive index profile. The remaining problem is to determine the power distribution over the eigenmode basis and be sure that the residues are virtually zero, which gives:

$$(\mathbf{M^P})^{\mathrm{T}}_{x,y,f} \times (\mathbf{R}\ )_{x,y,n} \cong 0\,. \quad (5)$$

With eq. (5) satisfied, eq. (4) reduces to:

$$(\mathbf{MF})_{f,n} = \left[(\mathbf{M^P})^{\mathrm{T}}_{x,y,f} \times (\mathbf{M^P})_{x,y,f}\right]^{-1} \times (\mathbf{M^P})^{\mathrm{T}}_{x,y,f} \times (\mathbf{B}\ )_{x,y,n} \quad (6)$$

Eq. (6) gives the eigenmode content in a very efficient manner. The validity of the results obtained through eq. (6) is to be checked according to eq. (5). Condition (5) can be evaluated as follows:

$$R_{dB} = 10 \times \log\left[1 - \frac{\iint \left|\mathbf{B}_{x,y} - (\mathbf{M^P})_{x,y,f} \times (\mathbf{MF})_f\right| dxdy}{\iint \mathbf{B}_{x,y}\, dxdy}\right] \quad (7)$$

Equation (7) evaluates in a convenient way the power loss induced by the reconstruction of the beam. A small value of residue is the main indicator that a modal analysis accurately represents the sampled modal composition.

2.3 Modal Interferences

The different eigenmodes propagating in a fiber interfere; therefore, the resulting output beam intensity depends on: (1) the wavelength, and (2) the fiber length. Since the different eigenmodes have different velocities, their relative phase is drifting with wavelength which produces beating of the modal interferences. This latter property is the basic principle supporting S^2I imaging.[3] The interference beat interval is related to the fiber length and modal velocity difference. The electric field interferences generate intensity I that can be written as follows:

$$\left.\frac{dI}{d\lambda}\right|_{\lambda} = i(\lambda)\left\{A_{01}^2 E_{01}^2 + \sum_{p\neq 01}^{q} A_p^2 E_p^2 + 2A_{01}E_{01}\sum_{p\neq 01}^{q} A_p \cos(\varphi_p) E_p + \sum_{p\neq 01}^{q}\sum_{r\neq 01}^{q} A_p A_r \cos(\varphi_p - \varphi_r) E_p E_r\right\} \quad (8)$$

In eq. (8) function of spatial localization (x, y), wavelength (λ), time (t) and propagation length (L) have been omitted for simplicity. The significant terms are: the wavelength varying phases φ_i related to the modal velocity difference with LP_{01} mode; the power source spectral density is: $i(\lambda)$; the modal electric field amplitudes are denoted A_i (considering the eigenmode electric fields to transport unit power).

IFA will be working properly to the desired accuracy by incorporating all the eigenmodes intensity distributions (E_p^2) and the eigenmode field cross product distributions ($E_p E_r$).

2.4 Interferences removal using a broad band source

Using a monochromatic source generates mode interferences that increase rapidly the number of components (eigenimages) necessary to perform IFA. The number of eigenimages including the field cross products necessary to perform IFA on a fiber that guides *n* eigenmodes at a specific wavelength is given by [*n*×(*n*+1)]/2. Increasing the number of image factors decreases the accuracy of the results when dealing with physical images containing: noise, limited intensity resolution and possible other perturbations. The two 1st terms in eq. (8) are wavelength independent; each of the other terms varies between a minimum and a maximum through the cosine function: these minimum and maximum almost do not depend on wavelength. Hence, integrating eq. (8) over a wavelength range will permit to reduce and even eliminate the wavelength dependent terms in eq. (8):

$$I = \int_{\lambda_0}^{\lambda_1} i(\lambda)\left[A_{01}^2 E_{01}^2 + \sum_{p\neq 01}^{q} A_p^2 E_p^2 + 2A_{01}E_{01}\sum_{p\neq 01}^{q} A_p \cos(\varphi_p)E_p + \sum_{p\neq 01}^{q}\sum_{r\neq 01,r}^{q} A_p A_r \cos(\varphi_p - \varphi_r)E_p E_r \right] d\lambda \qquad (9)$$

Separating the wavelength dependent terms, eq. (9) becomes:

$$I = \begin{cases} \left(A_{01}^2 E_{01}^2 + \sum_{p\neq 01}^{q} A_p^2 E_p^2 \right)\int_{\lambda_0}^{\lambda_1} i(\lambda)d\lambda \\ + \int_{\lambda_0}^{\lambda_1} i(\lambda)\left[2A_{01}E_{01}\sum_{p\neq 01}^{q} A_p \cos(\varphi_p)E_p + \sum_{p\neq 01}^{q}\sum_{r\neq 01}^{q} A_p A_r \cos(\varphi_p - \varphi_r)E_p E_r \right] d\lambda \end{cases} \qquad (10)$$

Equation (9) can be simplified if particular conditions are nearly fulfilled, namely: (i) The power is uniformly distributed over the wavelength range, that is: $i(\lambda) = I_1$; (ii) The field spatial distribution is nearly independent of wavelength; and (iii) The modal distribution is almost independent of wavelength (and total power);

Condition (i) can be fulfilled if the spectrum of the source only slowly varies with wavelength. Eq. (10) can be simplified into:

$$I = \begin{cases} I_1(\lambda_1 - \lambda_0)\times\left(A_{01}^2 E_{01}^2 + \sum_{p\neq 01}^{q} A_p^2 E_p^2 \right) \\ + 2I_1 A_{01}E_{01}\sum_{p\neq 01}^{q} A_p E_p \int_{\lambda_{p0}}^{\lambda_1} \cos(\varphi_p)d\lambda + I_1 \sum_{p\neq 01}^{q}\sum_{r\neq 0}^{q} A_p A_r E_p E_r \int_{\lambda_{pr0}}^{\lambda_1} \cos(\varphi_p - \varphi_r)d\lambda \end{cases} \qquad (11)$$

Where $[\lambda_{p0}, \lambda_1]$ and $[\lambda_{pr0}, \lambda_1]$ are small wavelength intervals. These represent a phase variation included in the $[0, 2\pi[$ interval that remains after subtracting every complete cycles of the cosine functions in eq. (10) over the entire interval $[\lambda_0, \lambda_1]$. The 1st line term in eq. (11) increases with the integration range. The 2nd line terms are oscillating between a minimum and a maximum that remain small compared to the 1st line value that increases continuously with the integration range. Provided that $[\lambda_1-\lambda_{p0}] << [\lambda_1-\lambda_0]$ and $[\lambda_1-\lambda_{pr0}] << [\lambda_1-\lambda_0]$ equation (11) reduces to:

$$I = I_1(\lambda_1 - \lambda_0)\times\left(A_{01}^2 E_{01}^2 + \sum_{p\neq 01}^{q} A_p^2 E_p^2 \right) \qquad (12)$$

Therefore, when $[\lambda_0, \lambda_1]$ is broad enough and the source intensity nearly flat, IFA can be performed using eq. (12) that is: the number of eigenimages required is by far smaller (*n*) instead of [*n*×(*n*+1)]/2. Reducing the size of eigenimages basis will increase the accuracy of the analysis of physical images. A limitation to this statement will be due to modes that possess similar velocity: their field cross product may not cancel by using a BBS ($\varphi_p - \varphi_r = 0$ in eq. 11). This however would give a second order intensity term when dealing with low HOM beam content.

3. SIMULATIONS

3.1 Limits related to intensity resolution

Simulation has been performed on the "pure" modes for a step index 27/250/0.115 fiber, that is: core radius R_{co} = 13.5 µm, and NA = 0.115.

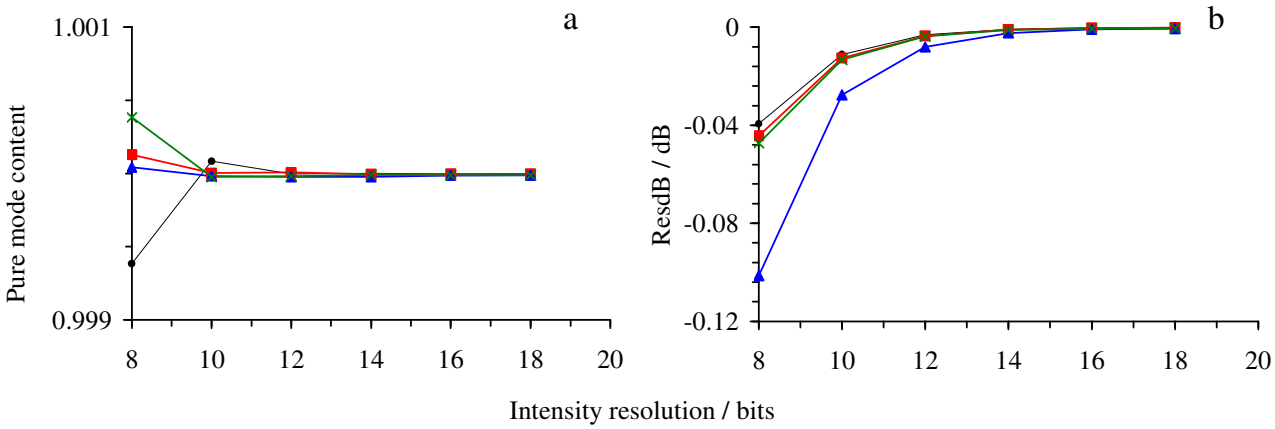

Figure 1 IFA of simulated eigenmodes as a function of intensity resolution (8–18 bits), LP_{01}, black circles; LP_{11}, red squares; LP_{02}, blue triangles; and LP_{21}, green X. (a) the mode content retrieved; and (b) loss due to the residuals.

The results indicate that an intensity resolution below 12 bits generates high residuals up to –0.10 dB at 8 bits and errors when using the field cross products in IFA (not shown). Errors were found to be related to the high similarity between $LP_{11} + LP_{11}^{T}$ and a combination of LP_{01} and cross product $E_{01} \times E_{02}$ that can be solved by using intensity resolution higher than 11 bits. The overall accuracy of the mode content retrieval by IFA is better than 0.02% with 12 bits and more resolution, with residual loss better than –0.01 dB (@ 12 bits).

3.2 Sensitivity to the wavelength selection for eigenmodes calculation

Using the same fiber, we found that residues increase linearly with the wavelength absolute difference between the actual one and the one selected for eigenmode calculations. Table 1 gives the residue slopes for selected modes for a step index 27/250/0.115 fiber.

Table 1. Slope of the loss of power through the residue as a function of wavelength difference.

Eigenmode	Residual slope
LP_{01}	–0.0005 dB/nm
LP_{11}	–0.0012 dB/nm
LP_{02}	–0.0024 dB/nm
LP_{21}	–0.0018 dB/nm

Numerical values in Table 1 certainly depend on the actual composition of the fiber: core diameter and NA as well as wavelength range.

3.3 Minimum length for using a BBS

To almost eliminate mode interferences by the use of a BBS, wavelength range $[\lambda_1, \lambda_2]$ and fiber length L must satisfy:

$$L = p \frac{\lambda_1 \lambda_2}{(\lambda_2 - \lambda_1) c \delta\varphi^u} \tag{13}$$

Where c is the speed of light in vacuum, p is an integer, and $\delta\varphi^u$ is the phase velocity difference between two interfering modes. $\delta\varphi^u$ can be theoretically evaluated from the physical characteristics of the fiber. The $\lambda_2 - \lambda_1$ term can be replaced

by the full width at half height (FWHH) of the BBS. Numerical results from eq. (13) depend on the fiber characteristics. We tested it with the above a step index 27/250/0.115 fiber. We obtained for LP_{11}: $\delta\varphi^u$ = 1.1 ps×m^{-1} @ 1.05 µm wavelength, the mode smallest value for this fiber. Using a BBS with FWHH = 10 nm on gets a minimum length equal to 0.4 m (p = 1). We tested this result with different mode composition. Figure 2 displays the results for a 50% LP_{01}, 6% LP_{11}, 40% LP_{02}, and 4% LP_{21} beam image simulated with a non uniform BBS in the 1030–1090 nm range. IFA was applied using eigenmodes calculated at 1045 nm.

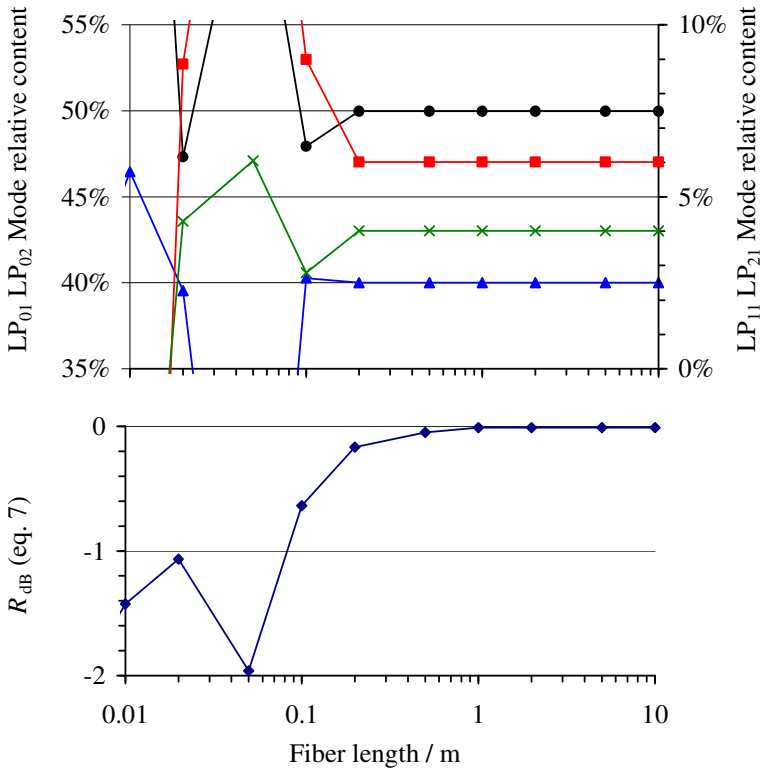

Figure 2 IFA of simulated beam image (50% LP_{01}, 6% LP_{11}, 40% LP_{02}, and 4% LP_{21}) as a function fiber length, LP_{01}, black circles; LP_{11}, red squares; LP_{02}, blue triangles; and LP_{21}, green X. Top the mode content retrieved LP_{01} and LP_{02} scale to the left, LP_{11} and LP_{21} scale to the right; and bottom loss due to the residues as an accuracy indicator.

IFA was applied not taking into account the mode interferences (that is: the mode fields cross products). Results shown in Figure 2 indicate that the mode content retrieved is correct even below the limiting fiber length 0.4 m. However, the residue loss is high due to the presence of residual mode interferences that are not taken into account in IFA. At the limiting length 0.4 m from eq. (13), results are accurate.

Notice that IFA using the field cross product profiles produces very accurate results even at low fiber length as expected from eq. (11) (results not shown).

4. EXPERIMENTAL RESULTS

The experimental setup consists of a 50X magnifying lens focused on the LMA fiber output cleave. The image from the lens is fed into a CCD of 9.9 × 9.9 µm pixel size. 5 to 30 images are averaged in order to reduce high speed source noise and variability. Image post processing includes basic operations such as centering, dimensional scaling and background removal. The proposed technique was successfully applied on two simple systems to prove concept.

4.1 HI1060 into SMF28 fibers: HOM produced by misalignment.

In the 1060 nm range a single mode fiber (HI1060) is fed into a bimodal one (SMF28) by means of a splicing machine. Input fiber was illuminated with broad band light in the 1040–1080 nm band. Six small steps of horizontal displacement

were programmed symmetrically about the optimum alignment position and output beam pictures recorded. Thus, from IFA we retrieved the resulting mode content (Fig. 3) showing that increasing misalignment increases the excitation of the LP_{11} mode to the expense of LP_{01} source mode. The LP_{11} excitation shows that both available orientations are simultaneously obtained to a similar extent as long as the displacement remains small, keeping the axial symmetry of the beam.

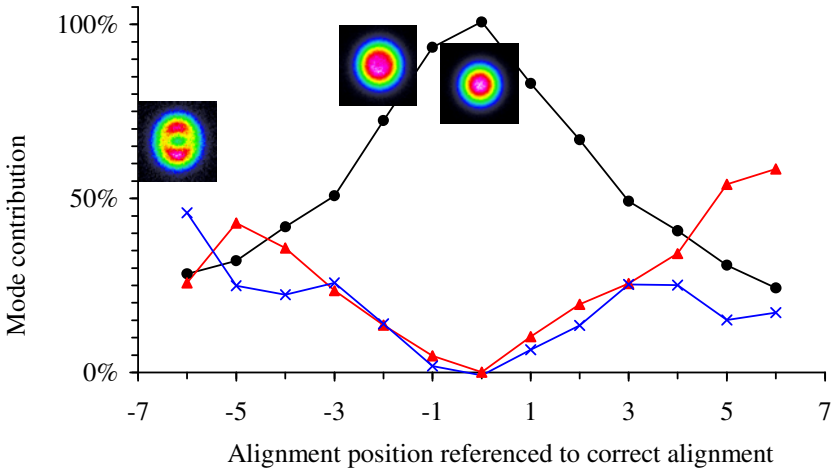

Figure 3 IFA results from small coaxial displacement between HI1060 and SMF28 butt coupled using a BBS source in the 1060 nm range. The relative mode content: LP_{01} full circles; LP_{11} both orientations full triangles and crosses. The three beam images are at –6, –2 and 0 positions, respectively, from auto alignment. Color intensity scale is used for maximum contrast.

4.2 Measurement of MFA: HI-1060–25/250/0.11

BBS injection in a single mode HI1060 connected to a MFA[5] feeding a multimode 25 µm core diameter, 0.11 numerical aperture LMA fiber. Such MFAs are used to bridge together fibers with mismatching mode diameters in order to maximize LP_{01} transmission (avoid HOM scattering). LP_{01} losses of less than 5% (–0.2 dB) are typically observed.[5] Figure 4 summarizes IFA results.

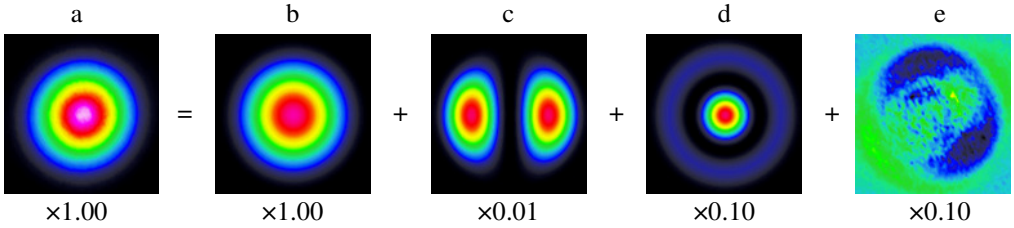

Figure 4 IFA typical experimental results. (a) Raw image of the LMA output facet; (b), (c), (d) Computed eigenimages associated to LP_{01}, LP_{11}, and LP_{02}, respectively; and (e) image residue. Low intensity (c), (d) and (e) images are presented on a distinct color scale, each having its own multiplying factor.

From IFA, it is found that this MFA is a good quality one:[5] LP_{01} transmission (Fig. 4b) largely dominates (95.8% of total transmitted power, –0.19 dB). LP_{11} carries virtually no power (Fig. 4c), while LP_{02} contributes 4.1% (Fig. 4d). The low amplitude residue (Fig. 4e) does not exhibit any of the fiber guided mode patterns.

5. CONCLUSION

IFA is a simple, low cost and high efficiency method to determine the mode content of a beam emerging from a few moded waveguide. It very well applies to near field measurements. Theoretical profiles can be obtained by solving the waveguide propagation equations or from direct experimental measurements. Method accuracy had been validated using beam simulations. Experimental measurement using a BBS in the 1060 nm range (FWHH = 10 nm) presented on (i)

commercial splicing machine auto alignment coupling HI-1060 and SMF28 fibers, and (ii) MFA from HI1060 to 25/250 NA=0.11 commercial fiber demonstrate the efficiency of the proposed method for precise beam quality analysis.

REFERENCES

[1] Yoda H., Polynkin P., Mansuripur M., "Beam Quality Factor of Higher Order Modes in a Step-Index Fiber", J. Lightwave Technol. **24**, 1350 (2006).

[2] Chan J.S.P., Wang P., Sahu J.K., Clarkson W.A., "Impact of Modal interference on the output Beam Properties of Large-Core Cladding-pumped Fiber Amplifiers", Opt. Soc. Am., CLEO/QELS, CWB4 (2008).

[3] Nicholson J.W., Yablon A.D., Ramachandran S., Ghalmi S., "Spatially and spectrally resolved imaging of modal content in large-mode-area fibers", Optic Express, **16** 7233 (2008)

[4] Wielandy S., "Implications of higher-order mode content in large mode area fiberrs with good beam quality", Optics Lett., **15**, 15402 (2007).

[5] Faucher M., Martineau L., Perreault R., Lizé Y. K., "Mode Field Adaptation for High power Fiber Lasers", CLEO proceedings CF17 (2007)

[6] Blin S., Nguyen T.N., Nguyen D.M., Rochard P., Provino L., Monteville A., Robin T., Mugnier A., Cadier B., Pureur D., Thual M., Chartier T., "New Methods for Modal Decomposition in Multi-Mode fibers", Proc. SPIE, **7503**, 750346 (2009).

[7] Bromage J., Dorrer C., Shoup M.J., Zuegel J.D., "Modal Measurement of a Large-Area Photonic Crystal Fiber Amplifier Using Spatially resolved Spectral Interferometry" (2009).

[8] Skorobogatiy M., Anastassiou C., Johnson S., Weisberg O., Engeness T., Jacobs S., Ahmad R., Fink Y., "Quantitative characterization of higher-order mode converters in weakly multimoded fibers," Opt. Express **11**(22), pp. 2838–2847, (2003).

[9] Fang H.-T., Huang D.-S., "Extracting mode components in laser intensity distribution by independent component analysis", Applied Optics, **44**, 3646 (2005).

[10] Malinowski, E. R.; Howery, D. G. *Factor analysis in chemistry*; Robert E Krieger Publishing Co: Malabar, Fl, 1989.

[11] Max J.-J., Chapados C., "Infrared spectroscopy of acetone-water liquid mixtures: I. Factor analysis", J. Chem. Phys. **119**, 5632 (2003); "Infrared spectroscopy of acetone-water liquid mixtures: II. Molecular Model", Ibid, **120**, 6625 (2004).

[12] Max J.-J., Gessinger V., Driessche C. van, Larouche P., Chapados C., "Infrared spectroscopy of aqueous ionic salt solutions at low concentrations", J. Chem. Phys., **126**, 184507 (2007).

[13] Max J.-J. Chapados C., "Infrared spectroscopy of aqueous carboxylic acids: comparison between acids and their salts", J. Phys. Chem. A **108**, 3324 (2004).

[14] Max J.-J. Chapados C., "Infrared spectroscopy of methanol-hexane liquid mixtures. II. The strength of hydrogen bondings", J. Chem. Phys. **130**, 124513 (2009) and references herein.

[15] Max J.-J. Chapados C., "Isotop effects in liquid water by infrared spectroscopy", J. Chem. Phys. **116**, 4626 (2002).